

Quantum Analytic Descent

Bálint Koczor* and Simon C. Benjamin

Department of Materials, University of Oxford, Parks Road, Oxford OX1 3PH, United Kingdom

Variational algorithms have particular relevance for near-term quantum computers but require non-trivial parameter optimisations. Here we propose Analytic Descent: Given that the energy landscape must have a certain simple form in the local region around any reference point, it can be efficiently approximated in its entirety by a classical model – we support these observations with rigorous, complexity-theoretic arguments. One can classically analyse this approximate function in order to directly ‘jump’ to the (estimated) minimum, before determining a more refined function if necessary. We verify our technique using numerical simulations: each analytic jump can be equivalent to many thousands of steps of canonical gradient descent.

An exciting era was heralded last year with the announcement of a quantum device whose behaviour cannot be simulated using classical computers with practical levels of resource [1]. In this era, quantum computers may have the potential to perform useful tasks of value. One very promising class of approaches are generically called quantum variational algorithms in which one seeks to make use of a quantum circuit of (presumably) relatively low depth [2–6], by adjusting the function it performs to tune it to the desired task.

Typically a simple-to-prepare reference state (such as all-zero) is passed into a quantum circuit, called the ansatz circuit, within which there are numerous parametrised gates. The idea exists in many variants, both theoretical and experimental [7–27]. In a typical implementation, each gate implements a unitary which is therefore also parameterised; for example $\exp(-i\theta\sigma_x/2)$, where σ_x is the Pauli X operator acting on a given qubit, and θ is the classical parameter. For a suitably-chosen ansatz circuit and an appropriate number of independently parametrised gates, the emerging state (also called the ansatz state) may be very complex – while inevitably being restricted to a small proportion of the exponentially large Hilbert space. Once a suitable ansatz circuit is chosen and it can be initialised in parameter space close to the desired state, the problem ultimately becomes one of parameter search.

A popular choice is gradient descent and, in particular, its more advanced variants, such as natural gradient [28, 29] which is closely related to imaginary time evolution [30]. Although much studied, gradient descent has its limitations and costs: Determining the energy of chemical systems, must be performed to a very high accuracy to be useful (e.g. chemical accuracy, equivalent to 3 or 4 decimal places [5]). This corresponds to finding the minimum of the energy landscape very perfectly, which is problematic since the gradients vanish and thus estimating them can become increasingly expensive due to shot noise [20, 31, 32].

In the present paper we study an alternative method: Using an ansatz circuit within which gates correspond

to Pauli strings (a universal construction), we observe that the cost function will necessarily have certain simple properties in the local region around any reference point. Exploiting this knowledge, we sample from the ansatz circuit to determine an analytic function to the near-minimum region. Given this function, we can descend towards the minimum classically and then take a ‘large jump’ (as compared to the small incremental steps taken in generic gradient descent) direct to that point. If necessary we then repeat the procedure of refining the analytic function and jumping again, until we reach a point satisfactorily close to the true minimum. In numerical simulations of this approach, we find that a single jump can be equivalent of thousands of steps of generic gradient descent.

Expanding the ansatz circuit—Quantum gates generated by Pauli strings have only two distinct eigenvalues, and it is straightforward to see that as we vary the parameter θ associated with such a gate, the corresponding slice of the energy surface is simply of the form $a + b \cos \theta + c \sin \theta$ for some $a, b, c \in \mathbb{R}$. For further discussion refer to [33–35].

It immediately follows from the above property that the Fourier spectrum of the full energy surface is determined by 3^ν coefficients, where ν is the number of parameters. Despite the very simple structure of such functions, determining them classically is intractable. Nevertheless, previous works proposed that the *exact* energy surface can be reconstructed for a classically tractable number of parameters, e.g., $\nu = 1, 2$, while freezing other parameters and thereby sequentially optimising the surface using a classical computer [36–38]. Such sequential optimisations are, however, vulnerable to getting stuck in local minima and can be expected to reach the optimum more slowly than gradient-based techniques, such as the natural gradient approach [28–30, 39]. Here we make the fundamental observation that one could efficiently obtain – by estimating only a quadratic number of terms – a good *classical approximation* of the full energy surface (and its full gradient vector) that is valid in the vicinity of any reference point. We support these observations with rigorous, complexity-theoretic arguments. Let us introduce our model.

We define an ansatz circuit as a CPTP mapping, and

* balint.koczor@materials.ox.ac.uk

in particular, as a product of individual gate operations that we write in terms of their superoperators as

$$\Phi(\underline{\theta}) := \Phi_\nu(\theta_\nu) \dots \Phi_2(\theta_2) \Phi_1(\theta_1). \quad (1)$$

Here $\Phi_k(\theta_k)$ are parameterised quantum gates. We focus on quantum gates which are generated by Pauli strings as (approximately) unitary operators $\Phi_k(\theta_k)\rho \approx U\rho U^\dagger$ with $U = \exp(-i\theta_k P_k/2)$. Here P_k are products of single-qubit Pauli operators as $P_k \in \{\text{Id}, \sigma_x, \sigma_y, \sigma_z\}^{\otimes N}$. For any such ansatz circuit, we can expand every gate into the following form. First, let us fix θ_0 and express the continuous dependence of the quantum gates on the angle θ around the fixed θ_0 as

$$\Phi_k(\theta_0 + \theta) = a(\theta)\Phi_{ak} + b(\theta)\Phi_{bk} + c(\theta)\Phi_{ck}, \quad (2)$$

where $a(\theta), b(\theta) = 1 \pm \cos(\theta)$ and $c(\theta) = \sin(\theta)/2$ are simple Fourier components. The transformations can be specified as $\Phi_{ak} = \Phi_k(\theta_0)$, and via parameter shifts as $\Phi_{bk} = \Phi_k(\theta_0 + \pi/2) - \Phi_k(\theta_0 - \pi/2)$ and $\Phi_{ck} = \Phi_k(\theta_0 + \pi)$. Note that these transformations are discrete in nature, and implicitly depend on the constant θ_0 which we have fixed as a reference point. Refer to Appendix for more details.

We now expand the full ansatz circuit from Eq. (1) into the above form assuming that all gates are generated by Pauli strings via Eq. (2). We again fix $\underline{\theta}_0$ and express the continuous dependence on $\underline{\theta}$ around this reference point in parameter space as

$$\Phi(\underline{\theta}_0 + \underline{\theta}) = \prod_{k=1}^{\nu} [a(\theta_k)\Phi_{ak} + b(\theta_k)\Phi_{bk} + c(\theta_k)\Phi_{ck}]. \quad (3)$$

The above product can be expanded into a sum of 3^ν terms, which is classically intractable. Nevertheless, in the following we aim to approximate this mapping via a polynomial number of *important* summands and discard the remaining, less important terms. In particular, we introduce $\delta := \|\underline{\theta}\|_\infty$, which denotes the absolute largest entry in the parameter vector. We will now expand the above quantum circuit into a quadratic number of terms in ν which introduces an error $\mathcal{O}(\sin^3 \delta)$. We stress that this is not a simple Taylor expansion of the objective function, but a truncation of a finite, multivariate trigonometric series.

We derive the explicit form of this approximate mapping in the Appendix as

$$\begin{aligned} \Phi(\underline{\theta}) = A(\underline{\theta})\Phi^{(A)} + \sum_{k=1}^{\nu} [B_k(\underline{\theta})\Phi_k^{(B)} + C_k(\underline{\theta})\Phi_k^{(C)}] \\ + \sum_{l>k}^{\nu} [D_{kl}(\underline{\theta})\Phi_{kl}^{(D)}] + \mathcal{O}(\sin^3 \delta). \end{aligned} \quad (4)$$

Here $A, B_k, C_k, D_{kl} : \mathbb{R}^\nu \mapsto \mathbb{R}$ are multivariate functions – in fact, monomials in $a(\theta), b(\theta)$ and $c(\theta)$ – and they multiply the discrete mappings as, e.g., $A(\underline{\theta})\Phi^{(A)}$. In conclusion, these monomials are products of simple univariate

trigonometric functions and they completely absorb the continuous dependence on the parameters $\underline{\theta}$.

Classically computing the entire energy surface—A large class of potential applications of variational quantum circuits assume a target function that corresponds to *linear mappings* of the form $E(\underline{\theta}) := \text{Tr}[\mathcal{H}\Phi(\underline{\theta})\rho_0]$, that can be used to model, e.g., the expected energy of a physical system when \mathcal{H} is a Hamiltonian. Although quantum natural gradient [29, 32, 40] allows for more general objective functions, here we only consider such linear mappings. This, nevertheless, still contains a large class of important applications, such as the variational quantum eigensolver.

Using our expansion in Eq. (4), we can express the entire energy surface explicitly as

$$\begin{aligned} E(\underline{\theta}) = A(\underline{\theta})E^{(A)} + \sum_{k=1}^{\nu} [B_k(\underline{\theta})E_k^{(B)} + C_k(\underline{\theta})E_k^{(C)}] \\ + \sum_{l>k}^{\nu} [D_{kl}(\underline{\theta})E_{kl}^{(D)}] + \mathcal{O}(\sin^3 \delta). \end{aligned} \quad (5)$$

Here $E^{(A)}, E_k^{(B)}, E_k^{(C)}, E_{kl}^{(D)} \in \mathbb{R}$ can be reconstructed by estimating the energy expectation value at discrete points in parameter space using a quantum device. For example, $E^{(A)} = \text{Tr}[\mathcal{H}\Phi^{(A)}\rho_0] = E(\underline{\theta}_0)$ is just the energy at the fixed point $\underline{\theta}_0$ and $E_k^{(C)}$ is obtained similarly by shifting the k^{th} parameter by π , refer to Appendix. As such, fully determining the above expansion requires one to estimate the coefficients by querying the energy expectation value at overall $Q = 1 + 2\nu^2 - 2\nu$ points.

Fig. 1(a) shows approximation errors obtained from a simulated ansatz circuit of 12 qubits. In our simulations we determined all the $Q = \mathcal{O}(\nu^2)$ coefficients and used them to compute the approximate energy via Eq. (5) at 1000 randomly generated points in parameter space. These randomly generated points are in the vicinity of our reference $\underline{\theta}_0$, which we choose to be close to the global optimum. We plot the approximation error as a function of the absolute largest entry in the parameter vector given by the norm $\delta = \|\underline{\theta}\|_\infty$. Fig. 1(a) confirms the error scaling $\mathcal{O}(\delta^3)$ and shows that our approximation is very good in practice, i.e., the error is smaller than 10^{-3} as long as the parameter vector norm $\|\underline{\theta}\|_\infty$ is smaller than 0.1. We further remark that in the Appendix we derive exact and approximate symmetries of the energy function around local minima; the objective function is approximately reflection symmetric via $E(\underline{\theta}) \approx E(-\underline{\theta})$ and exactly reflection symmetric along slices θ_k .

Classically computing the gradient—We derive the full analytic gradient of the approximate energy surface from Eq. (5) in the Appendix and propose an efficient classical algorithm for computing it for a given input $\underline{\theta}$. This has a classical computational complexity of $\mathcal{O}(\nu^3)$. We simulate an ansatz circuit of 12 qubits in Fig. 1(b) and compute the approximation error of the analytically calculated gradient vector. We quantify this error using the similarity measure as the normalised scalar product

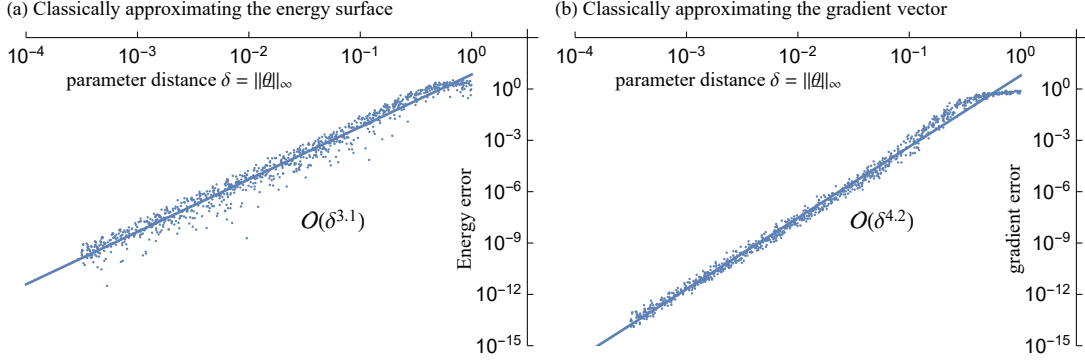


FIG. 1. Error of our trigonometric-series approximation for the entire energy surface (a) and gradient vector (b) as a function of the distance from the reference point $\underline{\theta}_0$ of our model. Distance $\delta = \|\underline{\theta}\|_\infty$ is given by the absolute largest entry in the parameter vector $\underline{\theta}$. As long as δ is small, we can classically approximate the gradient vector and use it in an analytic descent optimisation. The approximation error of the gradient vector is computed as the similarity measure $1 - f$, refer to text. We used the same spin-ring Hamiltonian and an 84-parameter ansatz circuit as in Fig. 2, and we have included the empirical scalings of the errors as $\mathcal{O}(\delta^{3.1})$ and $\mathcal{O}(\delta^{4.2})$.

$f = \langle \tilde{g} | g \rangle / (\|\tilde{g}\| \|g\|)$, between the exact g and the approximate \tilde{g} gradient vectors. We plot $1 - f$ in Fig. 1(b), and conclude that our approximation is very good and that our error measure scales with the parameter vector norm in fourth order as $1 - f = \mathcal{O}(\delta^4)$.

We aim to use this gradient in a classical optimisation routine (please refer to later text), but we first show that this approximation is very robust to shot noise. In particular, when using a quantum device to estimate the coefficients in Eq. (5), one needs to collect a large number of samples in order to sufficiently reduce the statistical uncertainty in those estimates. This uncertainty is quantified by the variance of the estimator, e.g., $\text{Var}[E_k^{(B)}]$ when reconstructing the coefficient $E_k^{(B)}$.

We derive the variance of the gradient estimator in the Appendix as

$$\text{Var}[\partial_m E(\underline{\theta})] = \left[\frac{\partial B_m(\underline{\theta})}{\partial \theta_m} \right]^2 \text{Var}[E_k^{(B)}] + \mathcal{O}(\sin^2 \delta). \quad (6)$$

This informs us that the variance of the classically computed gradient only depends on the variance of the coefficients $E_k^{(B)}$ in zeroth order – and the variance of all other estimated coefficients is scaled down quadratically by the possibly small $\delta \ll 1$. Note that the variance of our coefficients are directly proportional to the variance of estimating the energy expectation value as, e.g., $\text{Var}[E^{(A)}] = \text{Var}[E(\underline{\theta}_0)]$. Advanced techniques on reducing the variance of these energy expectation values can be straightforwardly applied, e.g., by simultaneously estimating commuting Pauli terms [41].

Metric tensors—We now show that our approximation of ansatz circuits in Eq. (3) can be used to obtain a classical model for computing how the quantum Fisher information matrix \mathbf{F}_Q depends on the continuous parameters $\underline{\theta}$. \mathbf{F}_Q reduces to other notions in special cases such as the Fubini-Study metric tensor and has been used extensively, e.g., in variational simulation or natural gradient

optimisation [14, 28–30, 42].

We derive the approximation of the general matrix elements $[\mathbf{F}_Q]_{mn}$ in the Appendix; for present purposes we need only state the leading terms explicitly as, e.g.,

$$[\mathbf{F}_Q]_{mn} = \mathcal{F}_{BB} F_{BB}(\underline{\theta}) + \mathcal{F}_{AB} F_{AB}(\underline{\theta}) + \dots \mathcal{O}(\sin^2 \delta). \quad (7)$$

Here the multi-variate trigonometric functions, e.g., $F_{BB}(\underline{\theta})$, can be straightforwardly computed using the previously outlined techniques. These functions multiply the real coefficients, such as \mathcal{F}_{BB} , which can be computed from quantum-state overlaps as

$$\begin{aligned} \mathcal{F}_{BB} = & \text{Tr}[\rho(\tfrac{1}{2}\pi v_k) \rho(\tfrac{1}{2}\pi v_k)] + \text{Tr}[\rho(-\tfrac{1}{2}\pi v_k) \rho(-\tfrac{1}{2}\pi v_k)] \\ & - \text{Tr}[\rho(-\tfrac{1}{2}\pi v_k) \rho(\tfrac{1}{2}\pi v_k)] - \text{Tr}[\rho(\tfrac{1}{2}\pi v_k) \rho(-\tfrac{1}{2}\pi v_k)]. \end{aligned}$$

These overlaps $\text{Tr}[\rho(\underline{\theta}') \rho(\underline{\theta}'')]$ correspond to variational states of shifted parameters $\underline{\theta}'$ and $\underline{\theta}''$, and can be estimated using SWAP tests or when the states are approximately pure as $\rho(\underline{\theta}) \approx |\psi(\underline{\theta})\rangle \langle \psi(\underline{\theta})|$, then the overlaps $|\langle \psi(\underline{\theta}') | \psi(\underline{\theta}'') \rangle|^2$ could be estimated via Hadamard tests. The latter would only require a single copy of the state.

Quantum Analytic Descent—Let us now propose our optimisation approach for variational quantum algorithms. We assume the aim is to optimise the objective function $E(\underline{\theta}) = \text{Tr}[\mathcal{H} \rho(\underline{\theta})]$, where we have again used the notation $\rho(\underline{\theta}) = \Phi(\underline{\theta}) \rho_0$. We use our classical approximation of the *entire* objective function $E(\underline{\theta})$ to descend towards its minimum using a classical computer. Our approach is therefore fundamentally different then previous ones since it alleviates the frequent use of a quantum computer (as opposed to, e.g., [36–38]) and moves more of the load to the classical machine.

We propose an iterative optimisation in two nested loops. In an external loop we use the quantum device to estimate the coefficients in Eq. (5). This allows us to build a classical model of the full objective function via Eq. (5). In the internal loop, we compute our classical

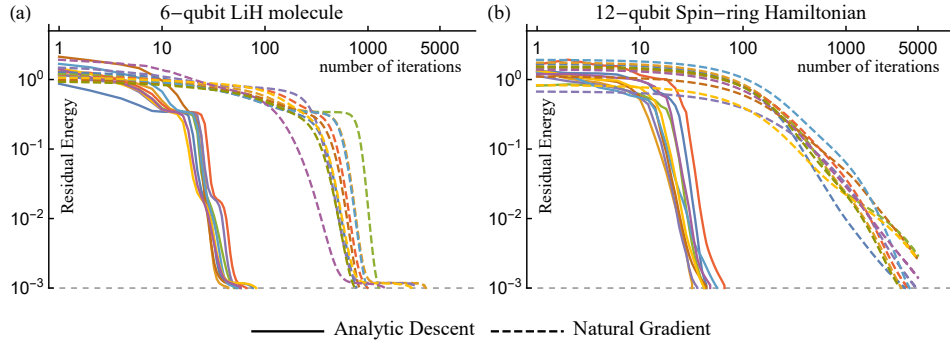


FIG. 2. Simulated analytic descent and natural gradient in the case of a molecular (a) and a spin-ring Hamiltonian (b). Logarithmic plots show the distance from the exact ground-state energy (Residual Energy) as a function of the iterations. A classical approximation of the entire energy surface is determined at each iteration step of analytic descent (solid lines) and in an internal loop we descent towards its minimum using a classical computer (not shown here). Analytic descent (solid lines) crucially outperforms conventional natural gradient (dashed lines) and appears to increase its convergence rate (steeper slope on plots). We simulate the effect of shot noise due to finite measurements – determining one step of analytic descent requires a factor of 2 more measurements (included in graphs) than natural gradient. Dashed grey lines show our convergence criterion 10^{-3} , which is comparable to chemical accuracy.

approximation of the gradient vector at every iteration step and propagate our parameters according to a suitable update rule. We choose quantum natural gradient [28–30] and although the metric tensor can similarly be approximated classically via Eq. (7), we remark that its quantum estimation cost becomes negligible in the vicinity of the optimum [32]. We use our efficient C implementation from [43] for computing the gradient vector classically: descending 1000 steps towards the minimum of the classical function can be performed in a matter of minutes on a single thread for up to many hundreds of parameters.

The internal, classical optimisation loop can be aided with feedback from the quantum device. There are various possibilities to implement this; one could estimate the energy with the quantum device occasionally, i.e., at every t iterations, and compare the result to the classical approximation. If the deviation is too large – possibly because $\|\theta\|_\infty$ is too large – then the internal loop should abort and the coefficients in Eq. (5) should be re-estimated using the quantum device. Another possibility for feedback would be to estimate the previously introduced similarity measure $1 - f$ between the approximate and exact gradients using the quantum device. In any case, we expect that this feedback from the quantum device only requires a negligible amount of sampling. One could of course work without feedback and abort the internal loop when $\|\theta\|_\infty$ exceeds a certain threshold.

Numerical simulations—We numerically simulate physical Hamiltonians. We consider a hardware-efficient ansatz construction which is built of alternating layers of single-qubit X and Y rotations and two-qubit Pauli ZZ gates. Refer to the Appendix for more details. We simulate the effect of shot noise in the following way. We set the number of measurements such that the precision

of each gradient entry is $\epsilon(g_k) = 0.1\|g\|/\sqrt{\nu}$. In order to be able to compare this to our analytic descent technique, we determine the coefficients to the same precision $\epsilon(E_k^{(B)}) = 0.1\|g\|/\sqrt{\nu}$ and we determine all other coefficients to a proportionally inferior precision $\epsilon = 0.1\|g\|$. Since our classical gradient estimator in Eq. (6) is dominated by the uncertainty in $E_k^{(B)}$, this way the overall number of measurements required for analytic descent is only a factor of 2 more than determining the gradient vector.

Fig. 2(a) shows simulation results of a LiH Hamiltonian of 6 qubits. We use an ansatz circuit with 4 blocks and overall 78 parameters. We start every optimisation from a randomly selected point in parameter space that is close to the Hartree-Fock solution. In Fig. 2(solid) we only plot the external optimisation loop of analytic descent. We plot curves that correspond to analytic descent in Fig. 2(solid) such that we propagate data points by 2 steps at every iteration – to reflect their relative measurement costs.

We have used a very fine step size in the case of analytical descent, which allows us to follow the natural gradient evolution of the parameters very smoothly ranging up to many thousands of conventional gradient steps per a single classical optimisation procedure (one iteration in Fig. 2). This small step size has many advantages, for example, it keeps the evolution stable even when the inverse of the ill-conditioned metric tensor \mathbf{F}_Q is applied to the gradient vector.

Fig. 2(b) shows simulation results of a spin-ring Hamiltonian. We have determined the ground state of this Hamiltonian using the previously introduced ansatz circuit, which consists of 2 blocks and overall 84 parameters. Analytic descent performs better than natural gradient even when being far from the optimum point. The gradi-

ent in this case is typically large and results in large steps that quickly drive away from the reference point θ_0 . Most importantly, both Fig. 2(a) and Fig. 2(b) confirm our expectations and we observe that analytic descent crucially outperforms natural gradient in the vicinity of the optimum. In some regions – especially when approaching the optimum – analytic descent even appears to result in an improved convergence rate (steeper slope in the figure).

Conclusion and Discussion—In this work we analytically determined how ansatz states depend on their parameters when all gates are generated by Pauli strings; although exponentially many coefficients determine a full trigonometric expansion, we propose an efficient, approximate approach for characterising the ansatz landscape in the vicinity of any reference point.

We derived explicit formulae for classically approximating the entire energy surface, the gradient vector and the metric tensor as a function of the ansatz parameters. This results in a novel hybrid quantum-classical optimisation scheme in which a quantum device is only occasionally used to determine a classical approximation of the entire energy surface. A classical optimisation routine is then used in an internal loop to descend towards the minimum of this approximate surface. As opposed to previous techniques – which relied on point-wise information – we use the explicit, analytic knowledge about the ansatz states to build a classically tractable model. We have outlined how our classical optimisation can be aided with occasional feedback from the quantum device.

We numerically simulated the ground-state search of physical Hamiltonians and observed that indeed analytical descent significantly outperforms conventional natural gradient. We have made our efficient C implementation of the classical gradient computation publicly available [43], which can be used in tandem with quantum simulators as well as with real quantum hardware.

There are a number of apparent, promising extensions. First, we could use the information from the previous iterations as a Bayesian prior when re-estimating our classical model in a next step. Second, we can similarly build a classical model of the metric tensor and compute it in the internal optimisation classically without using the quantum device. Third, one could sample the coefficients in Eq. (5) optimally by distributing samples according to their strengths [32]. Furthermore, during the internal op-

timisation loop, one could keep track of the variance of the gradient estimator, and if it becomes too sensitive to shot noise in only a few coefficients, one could collect specific targeted data with the quantum device without re-building the full model.

There are other interesting questions that we defer to future work. This includes a more detailed analysis of the effect of shot noise and other noise sources on analytic descent. We note that our approach is completely general and can be applied to any Hamiltonian \mathcal{H} , although, we expect that increasingly more complex Hamiltonians – such as in quantum chemistry – might result in more complex energy surfaces which are more difficult to approximate classically. The main advantage of our approach is that in all cases it guarantees an approximation error that scales with the fourth power of the distance from the reference point.

ACKNOWLEDGMENTS

SCB acknowledges financial support from EPSRC Hub grants under the agreement numbers EP/M013243/1 and EP/T001062/1, and from the IARPA funded LogiQ project. BK and SCB acknowledge funding received from EU H2020-FETFLAG-03-2018 under the grant agreement No 820495 (AQTION). The numerical modelling involved in this study made use of the Quantum Exact Simulation Toolkit (QuEST), and the recent development QuESTlink [44] which permits the user to use Mathematica as the integrated front end. The authors are grateful to those who have contributed to both these valuable tools. The views and conclusions contained herein are those of the authors and should not be interpreted as necessarily representing the official policies or endorsements, either expressed or implied, of the ODNI, IARPA, or the U.S. Government. The U.S. Government is authorized to reproduce and distribute reprints for Governmental purposes notwithstanding any copyright annotation thereon. Any opinions, findings, and conclusions or recommendations expressed in this material are those of the author(s) and do not necessarily reflect the view of the U.S. Army Research Office.

-
- [1] F. Arute, K. Arya, R. Babbush, and et al., Quantum supremacy using a programmable superconducting processor, *Nature* **574**, 505 (2019).
 - [2] I. Kassal, J. D. Whitfield, A. Perdomo-Ortiz, M.-H. Yung, and A. Aspuru-Guzik, Simulating chemistry using quantum computers, *Annual review of physical chemistry* **62**, 185 (2011).
 - [3] D. Lu, B. Xu, N. Xu, Z. Li, H. Chen, X. Peng, R. Xu, and J. Du, Quantum chemistry simulation on quantum computers: theories and experiments, *Phys. Chem. Chem. Phys.* **14**, 9411 (2012).
 - [4] K. B. Whaley, A. R. Dinner, and S. A. Rice, *Quantum information and computation for chemistry* (John Wiley & Sons, 2014).
 - [5] S. McArdle, S. Endo, A. Aspuru-Guzik, S. C. Benjamin, and X. Yuan, Quantum computational chemistry, *Rev. Mod. Phys.* **92**, 015003 (2020).
 - [6] B. Koczor, S. Endo, T. Jones, Y. Matsuzaki, and S. C. Benjamin, Variational-State Quantum Metrology, *New J. Phys.* **22**, 083038 (2020).

- [7] E. Farhi, J. Goldstone, and S. Gutmann, A quantum approximate optimization algorithm, arXiv preprint arXiv:1411.4028 (2014).
- [8] A. Peruzzo, J. McClean, P. Shadbolt, M.-H. Yung, Q. Zhou, P. J. Love, A. Aspuru-Guzik, and J. L. O'Brien, A variational eigenvalue solver on a photonic quantum processor, *Nature communications* **5** (2014).
- [9] Y. Wang, F. Dolde, J. Biamonte, R. Babbush, V. Bergholm, S. Yang, I. Jakobi, P. Neumann, A. Aspuru-Guzik, J. D. Whitfield, *et al.*, Quantum simulation of helium hydride cation in a solid-state spin register, *ACS nano* **9**, 7769 (2015).
- [10] P. J. J. O'Malley, R. Babbush, I. D. Kivlichan, J. Romero, J. R. McClean, R. Barends, J. Kelly, P. Roushan, A. Tranter, N. Ding, B. Campbell, Y. Chen, Z. Chen, B. Chiaro, A. Dunsworth, A. G. Fowler, E. Jeffrey, E. Lucero, A. Megrant, J. Y. Mutus, M. Neeley, C. Neill, C. Quintana, D. Sank, A. Vainsencher, J. Wenner, T. C. White, P. V. Coveney, P. J. Love, H. Neven, A. Aspuru-Guzik, and J. M. Martinis, Scalable Quantum Simulation of Molecular Energies, *Phys. Rev. X* **6**, 031007 (2016).
- [11] Y. Shen, X. Zhang, S. Zhang, J.-N. Zhang, M.-H. Yung, and K. Kim, Quantum implementation of the unitary coupled cluster for simulating molecular electronic structure, *Phys. Rev. A* **95**, 020501 (2017).
- [12] J. R. McClean, J. Romero, R. Babbush, and A. Aspuru-Guzik, The theory of variational hybrid quantum-classical algorithms, *New J. Phys.* **18**, 023023 (2016).
- [13] S. Paesani, A. A. Gentile, R. Santagati, J. Wang, N. Wiebe, D. P. Tew, J. L. O'Brien, and M. G. Thompson, Experimental Bayesian Quantum Phase Estimation on a Silicon Photonic Chip, *Phys. Rev. Lett.* **118**, 100503 (2017).
- [14] Y. Li and S. C. Benjamin, Efficient Variational Quantum Simulator Incorporating Active Error Minimization, *Phys. Rev. X* **7**, 021050 (2017).
- [15] J. I. Colless, V. V. Ramasesh, D. Dahlen, M. S. Blok, M. E. Kimchi-Schwartz, J. R. McClean, J. Carter, W. A. de Jong, and I. Siddiqi, Computation of Molecular Spectra on a Quantum Processor with an Error-Resilient Algorithm, *Phys. Rev. X* **8**, 011021 (2018).
- [16] R. Santagati, J. Wang, A. A. Gentile, S. Paesani, N. Wiebe, J. R. McClean, S. Morley-Short, P. J. Shadbolt, D. Bonneau, J. W. Silverstone, D. P. Tew, X. Zhou, J. L. O'Brien, and M. G. Thompson, Witnessing eigenstates for quantum simulation of Hamiltonian spectra, *Science Advances* **4**, 10.1126/sciadv.aap9646 (2018).
- [17] A. Kandala, A. Mezzacapo, K. Temme, M. Takita, M. Brink, J. M. Chow, and J. M. Gambetta, Hardware-efficient variational quantum eigensolver for small molecules and quantum magnets, *Nature* **549**, 242 (2017).
- [18] A. Kandala, K. Temme, A. D. Córcoles, A. Mezzacapo, J. M. Chow, and J. M. Gambetta, Error mitigation extends the computational reach of a noisy quantum processor, *Nature* **567**, 491 (2019).
- [19] C. Hempel, C. Maier, J. Romero, J. McClean, T. Monz, H. Shen, P. Jurcevic, B. P. Lanyon, P. Love, R. Babbush, A. Aspuru-Guzik, R. Blatt, and C. F. Roos, Quantum Chemistry Calculations on a Trapped-Ion Quantum Simulator, *Phys. Rev. X* **8**, 031022 (2018).
- [20] J. Romero, R. Babbush, J. R. McClean, C. Hempel, P. J. Love, and A. Aspuru-Guzik, Strategies for quantum computing molecular energies using the unitary coupled cluster ansatz, *Quantum Science and Technology* **4**, 014008 (2018).
- [21] O. Higgott, D. Wang, and S. Brierley, Variational Quantum Computation of Excited States, arXiv preprint arXiv:1805.08138 (2018).
- [22] J. R. McClean, M. E. Kimchi-Schwartz, J. Carter, and W. A. de Jong, Hybrid quantum-classical hierarchy for mitigation of decoherence and determination of excited states, *Physical Review A* **95**, 042308 (2017).
- [23] J. I. Colless, V. V. Ramasesh, D. Dahlen, M. S. Blok, J. R. McClean, J. Carter, W. A. de Jong, and I. Siddiqi, Robust determination of molecular spectra on a quantum processor, arXiv preprint arXiv:1707.06408 (2017).
- [24] C. Kokail, C. Maier, R. van Bijnen, T. Brydges, M. K. Joshi, P. Jurcevic, C. A. Muschik, P. Silvi, R. Blatt, C. F. Roos, *et al.*, Self-Verifying Variational Quantum Simulation of the Lattice Schwinger Model, arXiv preprint arXiv:1810.03421 (2018).
- [25] K. Sharma, S. Khatari, M. Cerezo, and P. J. Coles, Noise resilience of variational quantum compiling, *New Journal of Physics* **22**, 043006 (2020).
- [26] M. Cerezo, K. Sharma, A. Arrasmith, and P. J. Coles, Variational Quantum State Eigensolver, arXiv preprint arXiv:2004.01372 (2020).
- [27] B. Koczor, Exponential error suppression for Near-Term quantum devices, arXiv preprint arXiv:2011.05942 (2020).
- [28] J. Stokes, J. Izaac, N. Killoran, and G. Carleo, Quantum natural gradient, arXiv preprint arXiv:1909.02108 (2019).
- [29] B. Koczor and S. C. Benjamin, Quantum natural gradient generalised to non-unitary circuits, arXiv preprint arXiv:1912.08660 (2019).
- [30] S. McArdle, T. Jones, S. Endo, Y. Li, S. C. Benjamin, and X. Yuan, Variational ansatz-based quantum simulation of imaginary time evolution, *npj Quantum Information* **5**, 1 (2019).
- [31] A. Arrasmith, L. Cincio, R. D. Somma, and P. J. Coles, Operator Sampling for Shot-frugal Optimization in Variational Algorithms, arXiv preprint arXiv:2004.06252 (2020).
- [32] B. van Straaten and B. Koczor, Measurement cost of metric-aware variational quantum algorithms, arXiv preprint arXiv:2005.05172 (2020).
- [33] M. Schuld, V. Bergholm, C. Gogolin, J. Izaac, and N. Killoran, Evaluating analytic gradients on quantum hardware, *Phys. Rev. A* **99**, 032331 (2019).
- [34] J. G. Vidal and D. O. Theis, Calculus on parameterized quantum circuits, arXiv preprint arXiv:1812.06323 (2018).
- [35] M. Schuld, R. Sweke, and J. J. Meyer, The effect of data encoding on the expressive power of variational quantum machine learning models, arXiv preprint arXiv:2008.08605 (2020).
- [36] K. M. Nakanishi, K. Fujii, and S. Todo, Sequential minimal optimization for quantum-classical hybrid algorithms, *Phys. Rev. Research* **2**, 043158 (2020).
- [37] R. M. Parrish, J. T. Iosue, A. Ozaeta, and P. L. McMahon, A Jacobi diagonalization and Anderson acceleration algorithm for variational quantum algorithm parameter optimization, arXiv preprint arXiv:1904.03206 (2019).
- [38] M. Ostaszewski, E. Grant, and M. Benedetti, Quantum circuit structure learning, arXiv preprint

- arXiv:1905.09692 (2019).
- [39] D. Wierichs, C. Gogolin, and M. Kastoryano, Avoiding local minima in variational quantum eigensolvers with the natural gradient optimizer, arXiv preprint arXiv:2004.14666 (2020).
- [40] R. Sweke, F. Wilde, J. Meyer, M. Schuld, P. K. Fährmann, B. Meynard-Piganeau, and J. Eisert, Stochastic gradient descent for hybrid quantum-classical optimization, arXiv preprint arXiv:1910.01155 (2019).
- [41] O. Crawford, B. van Straaten, D. Wang, T. Parks, E. Campbell, and S. Brierley, Efficient quantum measurement of Pauli operators, arXiv preprint arXiv:1908.06942 (2019).
- [42] X. Yuan, S. Endo, Q. Zhao, Y. Li, and S. C. Benjamin, Theory of variational quantum simulation, *Quantum* **3**, 191 (2019).
- [43] B. Koczor, Quantum Analytic Descent, github.com/balintkoczor/quantum-analytic-descent (2020).
- [44] T. Jones and S. C. Benjamin, QuESTlink–Mathematica embiggened by a hardware-optimised quantum emulator, *Quantum Science and Technology* (2020).

Appendix A: Quantum gates generated by Pauli strings

1. Expressing a single gate

Let us consider a single gate in the ansatz circuit $U_k(\theta_k)$, where k indexes its position and $k \in \{1, 2, \dots, \nu\}$ with ν denoting the number of parameters. We assume that this gate is generated by a Pauli string P_k and ideally (when the gate is not noisy), it corresponds to the following unitary operator

$$U_k(\theta_k) := \exp(-i\theta_k P_k/2) = \cos[\theta_k/2] \text{Id} - i \sin[\theta_k/2] P_k, \quad (\text{A1})$$

where the second equality straightforwardly follows from the algebra $P_k^{2n} = \text{Id}$ and $P_k^{2n+1} = P_k$.

We now fix the parameter dependence of this gate at the reference point θ_0 and express the action of this gate on any quantum state using the continuous angle θ . Let us first define the quantum gate as a mapping $\Phi_k(\theta) : \mathcal{D} \mapsto \mathcal{D}$ over density operators, where \mathcal{D} denotes the set of density operators, i.e., positive, unit trace operators over the Hilbert space \mathbb{C}^{2^N} . The gate can then be expressed as a general mapping over arbitrary density matrices ρ as the unitary conjugation $U_k(\theta_0 + \theta)\rho U_k^\dagger(\theta_0 + \theta)$, and this can be expanded into the following transformations

$$\Phi_k(\theta)\rho := U_k(\theta)U_k(\theta_0)\rho U_k^\dagger(\theta_0)U_k^\dagger(\theta) = \cos^2[\theta_k/2]\rho_{ref} + \sin^2[\theta_k/2]P_k\rho_{ref}P_k - i \cos[\theta/2] \sin[\theta/2](P_k\rho_{ref} - \rho_{ref}P_k). \quad (\text{A2})$$

Here we have used the notation $\rho_{ref} := U_k(\theta_0)\rho U_k^\dagger(\theta_0)$. The dependency on the continuous angle θ is absorbed into the following functions

$$\begin{aligned} \cos[\theta/2]^2 &= (1 + \cos[\theta])/2, \\ \cos[\theta/2] \sin[\theta/2] &= \sin[\theta]/2, \\ \sin[\theta/2]^2 &= (1 - \cos[\theta])/2. \end{aligned}$$

We can now formalise Eq. (A2) by separating it into *discrete* mappings over density matrices which are multiplied by continuous functions that depend on the parameter θ as

$$\Phi_k(\theta) = a(\theta)\Phi_{ak} + b(\theta)\Phi_{bk} + c(\theta)\Phi_{ck}. \quad (\text{A3})$$

Here the mapping depends on the parameter θ via the Fourier components $a(\theta), b(\theta), c(\theta) : \mathbb{R} \mapsto \mathbb{R}$ and we define their explicit forms as

$$a(\theta) := (1 + \cos[\theta])/2 = \mathcal{O}(1 + \theta^2), \quad (\text{A4})$$

$$b(\theta) := \sin[\theta]/2 = \mathcal{O}(\theta), \quad (\text{A5})$$

$$c(\theta) := (1 - \cos[\theta])/2 = \mathcal{O}(\theta^2), \quad (\text{A6})$$

and we have also included their scaling when approaching $\theta \rightarrow 0$. Note that we have intentionally introduced the constant shift θ_0 and, of course, our definition corresponds to the action $\Phi_k(0)[\rho] = U_k(\theta_0)\rho U_k^\dagger(\theta_0)$ for the case $\theta \rightarrow 0$. The discrete mappings Φ_{ak}, Φ_{bk} and Φ_{ck} in Eq. (A3) can be specified via their action on arbitrary density matrices as

$$\begin{aligned} \Phi_{ak} \rho &= U_k(\theta_0)\rho U_k^\dagger(\theta_0) \equiv \Phi_k(0)\rho, \\ \Phi_{bk} \rho &= -i[P_k, U_k(\theta_0)\rho U_k^\dagger(\theta_0)] = -\frac{\partial \left(U_k(\theta)U_k(\theta_0)\rho U_k^\dagger(\theta_0)U_k^\dagger(\theta) \right)}{\partial \theta} \Big|_{\theta=0} \\ &= U_k(\theta_0 + \pi/2)\rho U_k^\dagger(\theta_0 + \pi/2) - U_k(\theta_0 - \pi/2)\rho U_k^\dagger(\theta_0 - \pi/2) \equiv [\Phi_k(\pi/2) - \Phi_k(-\pi/2)]\rho, \\ \Phi_{ck} \rho &= P_k U_k(\theta_0)\rho U_k^\dagger(\theta_0) P_k^\dagger = U_k(\theta_0 + \pi)\rho U_k^\dagger(\theta_0 + \pi) \equiv \Phi_k(\pi)\rho. \end{aligned}$$

We finally conclude by recollecting their explicit forms as

$$\Phi_{ak} = \Phi_k(0), \quad \Phi_{bk} = \Phi_k(\pi/2) - \Phi_k(-\pi/2), \quad \Phi_{ck} = \Phi_k(\pi). \quad (\text{A7})$$

We can use the above expressions to express any linear mapping, such as the energy functional $\mathcal{E}(\rho) : \mathcal{D} \mapsto \mathbb{R}$, via the trace relation $\mathcal{E}(\rho) = \text{Tr}[\mathcal{H}^\dagger \rho]$, which is often referred to as an expectation value, and \mathcal{H} is any Hermitian operator in the Hilbert space \mathbb{C}^{2^N} . We now consider the parametric mapping $E(\theta) : \mathbb{R} \mapsto \mathbb{R}$, which we define as $E(\theta) := [\mathcal{E} \circ \Phi_k(\theta)]\rho_0 = \mathcal{E}(\Phi_k(\theta)\rho_0)$ and we refer to it as the energy function, or energy landscape. The reference state can be, e.g., the computational zero state $\rho_0 := |\underline{0}\rangle\langle\underline{0}|$. We can express the energy function explicitly via the following Fourier series

$$E(\rho) = \text{Tr}[\mathcal{H} \Phi_k(\theta)\rho_0] = \alpha_k a(\theta) + \beta_k b(\theta) + \gamma_k c(\theta). \quad (\text{A8})$$

The Fourier coefficients $\alpha_k, \beta_k, \gamma_k \in \mathbb{R}$ can be completely determined by discrete samples of the energy function via the discrete mappings of the density matrix as

$$\alpha_k := \text{Tr}[\mathcal{H} \Phi_{ak}\rho_0] = E(0) + E(\pi) \quad (\text{A9})$$

$$\beta_k := \text{Tr}[\mathcal{H} \Phi_{bk}\rho_0] = E(\pi) \quad (\text{A10})$$

$$\gamma_k := \text{Tr}[\mathcal{H} \Phi_{ck}\rho_0] = E(\pi/2) - E(-\pi/2). \quad (\text{A11})$$

The above formula informs us that we can completely and analytically determine the full energy function $E(\theta)$, just by querying the function $E(\theta)$ at four different points as $(-\pi/2, 0, \pi/2, \pi)$. Of course Nyquist's theorem also informs us that this is suboptimal, since the Fourier spectrum of $E(\theta)$ is bounded with only 3 frequency terms present $(-1, 0, 1)$. This guarantees that querying the function $E(\theta)$ at only 3 points would be sufficient for completely reconstructing it. Note that due to our definitions, the parameter θ is shifted by the constant θ_0 and, for example, $E(0) = \text{Tr}[\mathcal{H} U_k(\theta_0)\rho_0 U_k^\dagger(\theta_0)]$.

2. Expanding the full ansatz circuit

Let us now consider the effect of the full ansatz circuit on the reference state $\rho_0 := |\underline{0}\rangle\langle\underline{0}|$ as

$$U(\underline{\theta}_0 + \underline{\theta})\rho_0 U^\dagger(\underline{\theta}_0 + \underline{\theta}), \quad \text{with} \quad U(\underline{\theta}_0 + \underline{\theta}) := U_\nu(\theta_{0,\nu} + \theta_\nu) \cdots U_2(\theta_{0,2} + \theta_2) U_1(\theta_{0,1} + \theta_1).$$

Here $\underline{\theta}_0 \in \mathbb{R}^\nu$ is a vector that represents a fixed, constant shift of the parameters, while the circuit depends continuously on the parameters $\underline{\theta} \in \mathbb{R}^\nu$.

Using results from the previous subsection, we can build an analytical model of the superoperator representation $\Phi(\underline{\theta})$ of the full ansatz circuit as the mapping

$$\Phi(\underline{\theta}) := \Phi_\nu(\theta_\nu) \cdots \Phi_2(\theta_2) \Phi_1(\theta_1) = \prod_{k=1}^\nu [a(\theta_k) \Phi_{ak} + b(\theta_k) \Phi_{bk} + c(\theta_k) \Phi_{ck}]. \quad (\text{A12})$$

The above equation expresses the full ansatz circuit and its dependence on the parameters $\underline{\theta}$. Of course fully expanding the above expression would result in a sum of 3^ν different terms. Nevertheless, we expand this into a sum and truncate the expansion such that the remaining terms are correct up to an error $\mathcal{O}(\sin^3 \delta)$. For this we define $\delta := \|\underline{\theta}\|_\infty$, to denote the absolute largest entry in the vector $\underline{\theta}$. We assume that the continuous parameters are only used to explore the vicinity of the reference point $\underline{\theta}_0$ in parameter space via a sufficiently small δ . This can be, e.g., when the reference parameters $\underline{\theta}_0$ are already a good approximation of the optimal ones as $\|\underline{\theta}_0 - \underline{\theta}_{opt}\|_\infty < \delta$ with $\delta \ll 1$ and we search for the ground state energy by optimising the continuous parameters. We define the approximate mapping as

$$\tilde{\Phi}(\underline{\theta}) := A(\underline{\theta}) \Phi^{(A)} + \sum_{k=1}^\nu [B_k(\underline{\theta}) \Phi_k^{(B)} + C_k(\underline{\theta}) \Phi_k^{(C)}] + \sum_k \sum_{l=k+1}^\nu [D_{kl}(\underline{\theta}) \Phi_{kl}^{(D)}]. \quad (\text{A13})$$

Here the functions $A(\underline{\theta})$, $B_k(\underline{\theta})$, $C_k(\underline{\theta})$ and $D_{kl}(\underline{\theta})$ absorb the dependence on the parameters $\underline{\theta}$ and $\Phi_k^{(A)}$, $\Phi_k^{(B)}$, $\Phi_k^{(C)}$ and $\Phi_{kl}^{(D)}$ are superoperators of discrete mappings. We compute the explicit form of the terms appearing in the

summation in Eq. (A13) as

$$\begin{aligned}
A(\underline{\theta}) \times \Phi^{(A)} &= \prod_{k=1}^{\nu} [a(\theta_k) \Phi_{ak}] = \mathcal{O}(1), \\
B_k(\underline{\theta}) \times \Phi_k^{(B)} &= [a(\theta_{\nu}) a(\theta_{\nu-1}) \cdots b(\theta_k) \cdots a(\theta_2) a(\theta_1)] \times [\Phi_{a\nu} \Phi_{a(\nu-1)} \cdots \Phi_{bk} \cdots \Phi_{a2} \Phi_{a1}] = \mathcal{O}(\theta_k), \\
C_k(\underline{\theta}) \times \Phi_k^{(C)} &= [a(\theta_{\nu}) a(\theta_{\nu-1}) \cdots c(\theta_k) \cdots a(\theta_2) a(\theta_1)] \times [\Phi_{a\nu} \Phi_{a(\nu-1)} \cdots \Phi_{ck} \cdots \Phi_{a2} \Phi_{a1}] = \mathcal{O}(\theta_k^2), \\
D_{kl}(\underline{\theta}) \times \Phi_{kl}^{(D)} &= \left([a(\theta_{\nu}) \Phi_{a\nu}] \cdots [b(\theta_k) \Phi_{ck}] \cdots [b(\theta_l) \Phi_{cl}] \cdots [a(\theta_1) \Phi_{a1}] \right) = \mathcal{O}(\theta_k \theta_l).
\end{aligned}$$

The discrete mappings can be further simplified by using Eq. (A7) as

$$\Phi^{(A)} = \Phi(\underline{0}), \quad \Phi_k^{(B)} = \Phi(\frac{1}{2}\pi \underline{v}_k) - \Phi(-\frac{1}{2}\pi \underline{v}_k), \quad \Phi_k^{(C)} = \Phi(\pi \underline{v}_k) \quad (\text{A14})$$

$$\Phi_{kl}^{(D)} = \Phi(\frac{1}{2}\pi \underline{v}_k + \frac{1}{2}\pi \underline{v}_l) + \Phi(-\frac{1}{2}\pi \underline{v}_k - \frac{1}{2}\pi \underline{v}_l) - \Phi(-\frac{1}{2}\pi \underline{v}_k + \frac{1}{2}\pi \underline{v}_l) - \Phi(\frac{1}{2}\pi \underline{v}_k - \frac{1}{2}\pi \underline{v}_l), \quad (\text{A15})$$

where $\underline{v}_k \in \mathbb{R}^{\nu}$ denotes the standard basis vector, e.g., $(0, 0, \dots, 0, 1, 0, \dots, 0)$. We further remark that due to our definitions, the parameters $\underline{\theta}$ are shifted by the constant vector $\underline{\theta}_0$ and, for example, $\Phi(\underline{0})\rho_0 = U(\underline{\theta}_0)\rho_0 U^\dagger(\underline{\theta}_0)$.

We can quantify the error of the approximate mapping in Eq. (A13) via the trace distance of the resulting density operators and we express this as $\|\Phi(\underline{\theta})\rho - \tilde{\Phi}(\underline{\theta})\rho\|_{tr} = \mathcal{O}(\sin^3 \delta)$. We remark that our expansion in Eq. (A13) consist of a sum of $1 + \nu + \nu^2/2$ different terms and describes the variational mapping up to an error $\mathcal{O}(\sin^3 \delta)$. We could similarly expand the mapping into a sum of $\mathcal{O}(\nu^3)$ terms and have an error $\mathcal{O}(\sin^4 \delta)$ or beyond.

Appendix B: Approximating the full energy surface locally

We can express the full energy surface following our definition in the previous section and evaluating the discrete mappings

$$E(\underline{\theta}) := \text{Tr}[\mathcal{H} \Phi(\underline{\theta})\rho_0] = A(\underline{\theta})E^{(A)} + \sum_{k=1}^{\nu} [B_k(\underline{\theta})E_k^{(B)} + C_k(\underline{\theta})E_k^{(C)}] + \sum_k \sum_{l=k+1}^{\nu} [D_{kl}(\underline{\theta})E_{kl}^{(D)}] + \mathcal{O}(\sin^3 \delta). \quad (\text{B1})$$

We can express the discrete mappings as queries of the energy function at discrete points in parameter space as

$$\begin{aligned}
E^{(A)} &= \text{Tr}[\mathcal{H} \Phi^{(A)}\rho_0] = E(\underline{0}) \\
E_k^{(B)} &= \text{Tr}[\mathcal{H} \Phi_k^{(B)}\rho_0] = E(\frac{1}{2}\pi \underline{v}_k) - E(-\frac{1}{2}\pi \underline{v}_k) \\
E_k^{(C)} &= \text{Tr}[\mathcal{H} \Phi_k^{(C)}\rho_0] = E(\pi \underline{v}_k) \\
E_{kl}^{(D)} &= \text{Tr}[\mathcal{H} \Phi_{kl}^{(D)}\rho_0] = E(\frac{1}{2}\pi \underline{v}_k + \frac{1}{2}\pi \underline{v}_l) + E(-\frac{1}{2}\pi \underline{v}_k - \frac{1}{2}\pi \underline{v}_l) - E(-\frac{1}{2}\pi \underline{v}_k + \frac{1}{2}\pi \underline{v}_l) - E(\frac{1}{2}\pi \underline{v}_k - \frac{1}{2}\pi \underline{v}_l).
\end{aligned}$$

Here $\underline{v}_k \in \mathbb{R}^{\nu}$ denotes a standard basis vector, e.g., $(0, 0, \dots, 0, 1, 0, \dots, 0)$. Note that due to our definitions, the parameters $\underline{\theta}$ are shifted by the constant vector $\underline{\theta}_0$ and, for example, $E(\underline{0}) = \text{Tr}[\mathcal{H} U(\underline{\theta}_0)\rho_0 U^\dagger(\underline{\theta}_0)]$.

Using the above expressions, one can determine an $\mathcal{O}(\sin^3 \delta)$ approximation of the full energy surface by querying the energy function $E(\underline{\theta})$ at a total number of Q points, where

$$Q = 1 + \nu + 2\nu + 4(\nu^2/2 - \nu) = 1 + 2\nu^2 - 2\nu. \quad (\text{B2})$$

1. Expressing the gradient analytically

We now derive the dependence of the gradient vector components $g_m := \partial_m E(\underline{\theta})$ on the parameters $\underline{\theta}$ using our approximation from Eq. (B1). We can explicitly write

$$\partial_m E(\underline{\theta}) = \frac{\partial A(\underline{\theta})}{\partial \theta_m} E^{(A)} + \sum_{k=1}^{\nu} \left[\frac{\partial B_k(\underline{\theta})}{\partial \theta_m} E_k^{(B)} + \frac{\partial C_k(\underline{\theta})}{\partial \theta_m} E_k^{(C)} \right] + \sum_k \sum_{l=k+1}^{\nu} \left[\frac{\partial D_{kl}(\underline{\theta})}{\partial \theta_m} E_{kl}^{(D)} \right] + \mathcal{O}(\sin^2 \delta). \quad (\text{B3})$$

Let us first compute the derivatives of the single-variate functions from Eq. (A4) as

$$\frac{\partial a(\theta_k)}{\partial \theta_k} = -\sin[\theta_k]/2, \quad \frac{\partial b(\theta_k)}{\partial \theta_k} = \cos[\theta_k]/2, \quad \frac{\partial c(\theta_k)}{\partial \theta_k} = \sin[\theta_k]/2.$$

We now express the explicit forms compute partial derivatives of the monomials in the following. The first term is

$$\frac{\partial A(\underline{\theta})}{\partial \theta_m} = a(\theta_\nu) a(\theta_{\nu-1}) \cdots \frac{\partial a(\theta_m)}{\partial \theta_m} \cdots a(\theta_2) a(\theta_1) = \mathcal{O}(\theta_m).$$

Similarly we have

$$\frac{\partial B_k(\underline{\theta})}{\partial \theta_m} = \begin{cases} a(\theta_\nu) a(\theta_{\nu-1}) \cdots \frac{\partial b(\theta_m)}{\partial \theta_m} \cdots a(\theta_2) a(\theta_1) = \mathcal{O}(1) & \text{if } k = m \\ a(\theta_\nu) a(\theta_{\nu-1}) \cdots b(\theta_k) \cdots \frac{\partial a(\theta_m)}{\partial \theta_m} \cdots a(\theta_2) a(\theta_1) = \mathcal{O}(\theta_m \theta_k) & \text{if } k \neq m, \end{cases} \quad (\text{B4})$$

but note that here we do not not assume that $k > l$. Very similarly we have

$$\frac{\partial C_k(\underline{\theta})}{\partial \theta_m} = \begin{cases} a(\theta_\nu) a(\theta_{\nu-1}) \cdots \frac{\partial c(\theta_m)}{\partial \theta_m} \cdots a(\theta_2) a(\theta_1) = \mathcal{O}(\theta_m) & \text{if } k = m \\ a(\theta_\nu) a(\theta_{\nu-1}) \cdots c(\theta_k) \cdots \frac{\partial a(\theta_m)}{\partial \theta_m} \cdots a(\theta_2) a(\theta_1) = \mathcal{O}(\theta_m \theta_k^2) & \text{if } k \neq m, \end{cases} \quad (\text{B5})$$

and we again do not not assume that $k > l$. Finally,

$$\frac{\partial D_{kl}(\underline{\theta})}{\partial \theta_m} = \begin{cases} a(\theta_\nu) a(\theta_{\nu-1}) \cdots \frac{\partial b(\theta_m)}{\partial \theta_m} \cdots b(\theta_l) \cdots a(\theta_2) a(\theta_1) = \mathcal{O}(\theta_m) & \text{if } k = m \\ a(\theta_\nu) a(\theta_{\nu-1}) \cdots b(\theta_k) \cdots \frac{\partial b(\theta_m)}{\partial \theta_m} \cdots a(\theta_2) a(\theta_1) = \mathcal{O}(\theta_m) & \text{if } l = m \\ a(\theta_\nu) a(\theta_{\nu-1}) \cdots b(\theta_k) \cdots b(\theta_l) \cdots \frac{\partial a(\theta_m)}{\partial \theta_m} \cdots a(\theta_2) a(\theta_1) = \mathcal{O}(\theta_k \theta_l \theta_m) & \text{if } k \neq m \neq l. \end{cases} \quad (\text{B6})$$

One can therefore compute the full gradient vector analytically, up to an error $\mathcal{O}(\sin^2 \delta)$, via the monomials $A(\underline{\theta})$, $B_k(\underline{\theta})$, $C_k(\underline{\theta})$ and $D_{kl}(\underline{\theta})$. and the corresponding energy coefficients. These coefficients can be determined by querying the energy function at $\mathcal{O}(\nu^2)$ points as discussed in Sec. B. We propose an efficient classical algorithm for computing the this gradient vector, and its computational complexity is $\mathcal{O}(\nu^3)$, refer to Sec. D 1.

2. Error propagation and variances

Using a straightforward linear error propagation formula, the variance of the gradient estimator can be computed via the following terms

$$\begin{aligned} \text{Var}[\partial_m E(\underline{\theta})] &= \left[\frac{\partial A(\underline{\theta})}{\partial \theta_m} \right]^2 \text{Var}[E^{(A)}] + \sum_{k=1}^{\nu} \left(\left[\frac{\partial B_k(\underline{\theta})}{\partial \theta_m} \right]^2 \text{Var}[E_k^{(B)}] + \left[\frac{\partial C_k(\underline{\theta})}{\partial \theta_m} \right]^2 \text{Var}[E_k^{(C)}] \right) \\ &\quad + \sum_k \sum_{l=k+1}^{\nu} \left(\left[\frac{\partial D_{kl}(\underline{\theta})}{\partial \theta_m} \right]^2 \text{Var}[E_{kl}^{(D)}] \right) + \mathcal{O}(\sin^4 \delta). \end{aligned}$$

Here the variances, such as $\text{Var}[E^{(A)}] = \text{Var}[E(\underline{0})]$, are directly proportional to the precision of the energy estimation. This variance scales inversely with how many times the energy estimator is sampled.

Now using the scaling of the multivariate functions from B 1, we can expand the above variance into a leading term $\left[\frac{\partial B_m(\underline{\theta})}{\partial \theta_m} \right]^2 = \mathcal{O}(1)$ and into terms that scale with δ as

$$\text{Var}[\partial_m E(\underline{\theta})] = \left[\frac{\partial B_m(\underline{\theta})}{\partial \theta_m} \right]^2 \text{Var}[E_k^{(B)}] + \mathcal{O}(\sin^2 \delta).$$

As long as the norm $\|\underline{\theta}\|_\infty < \delta$ is sufficiently small, the variance of the gradient vector is dominated by the variances of measuring $\text{Var}[E_k^{(B)}]$. This means that, even though one has to query the energy function at $\mathcal{O}(\nu^2)$ points, most of these queries need not be very precise. In fact, the variance of the gradient component is dominated by the precision of the $\mathcal{O}(\nu)$ queries used to determine the coefficients $E_k^{(B)}$. Conversely, the measurement cost of estimating our classical model to a high precision is dominated by estimating the coefficients $E_k^{(B)}$.

3. Relation to the gradient vector and to the Hessian matrix

One can straightforwardly show that the coefficients used to determine our approximation of the energy surface are related to partial derivatives of the energy surface. In particular, the gradient vector g_m from Eq. (B3) can be

expressed exactly at the point $\underline{\theta}$ as

$$g_m = [\partial_m E(\underline{\theta})]|_{\underline{\theta}=\underline{0}} = E_m^{(B)} \left[\frac{\partial B_m(\underline{\theta})}{\partial \theta_m} \right] |_{\underline{\theta}=\underline{0}} = E_m^{(B)} / 2 = [E(\frac{1}{2}\pi v_k) - E(-\frac{1}{2}\pi v_k)] / 2. \quad (\text{B7})$$

This is the well-known parameter-shift rule, which estimates the gradient via sampling the energy function at two different points [33].

The mixed second partial derivatives can similarly be expressed exactly using Eq. (B1) as

$$[\partial_m \partial_n E(\underline{\theta})]|_{\underline{\theta}=\underline{0}} = E_{kl}^{(D)} \left[\frac{\partial^2 D_{kl}(\underline{\theta})}{\partial \theta_m \partial \theta_n} \right] |_{\underline{\theta}=\underline{0}} = E_{kl}^{(D)} / 4 \quad (\text{B8})$$

$$= [E(\frac{1}{2}\pi v_k + \frac{1}{2}\pi v_l) + E(-\frac{1}{2}\pi v_k - \frac{1}{2}\pi v_l) - E(-\frac{1}{2}\pi v_k + \frac{1}{2}\pi v_l) - E(\frac{1}{2}\pi v_k - \frac{1}{2}\pi v_l)] / 4, \quad (\text{B9})$$

when $n \neq m$ and

$$[\partial_m \partial_m E(\underline{\theta})]|_{\underline{\theta}=\underline{0}} = E^{(A)} \left[\frac{\partial^2 A(\underline{\theta})}{\partial \theta_m \partial \theta_m} \right] |_{\underline{\theta}=\underline{0}} + E_m^{(C)} \left[\frac{\partial^2 C_m(\underline{\theta})}{\partial \theta_m \partial \theta_m} \right] |_{\underline{\theta}=\underline{0}} \quad (\text{B10})$$

$$= [E_m^{(C)} - E^{(A)}] / 2 = E(\pi v_k) - E(\underline{0}). \quad (\text{B11})$$

To conclude, we express explicitly elements of the gradient vector as

$$g_m = [\partial_m E(\underline{\theta})]|_{\underline{\theta}=\underline{0}} = E_m^{(B)} / 2 \quad (\text{B12})$$

and elements of the Hessian matrix as

$$H_{mn} = [\partial_m \partial_n E(\underline{\theta})]|_{\underline{\theta}=\underline{0}} = \begin{cases} [E_m^{(C)} - E^{(A)}] / 2 & \text{if } m = n \\ E_{kl}^{(D)} / 4 & \text{if } m \neq n. \end{cases} \quad (\text{B13})$$

This means that when querying the energy function in Sec. B and in Sec. B 1, the information we determine is very closely related to the Hessian and the gradient of the energy surface. However, we stress that our approximation is not a simple Taylor expansion.

4. Symmetry of the energy surface around the optimum

At a local optimum one finds that the gradient vanishes as $g_m = 0$ for $m \in \{1, \dots, \nu\}$. We set $\underline{\theta}_0 := \underline{\theta}_{opt}$ and therefore $\underline{\theta} = \underline{0}$. The explicit form of the leading terms in the energy surface can be expressed as

$$E(\underline{\theta}) := \text{Tr}[\mathcal{H} \Phi(\underline{\theta}) \rho_0] = A(\underline{\theta}) E^{(A)} + \sum_{k=1}^{\nu} [C_k(\underline{\theta}) E_k^{(C)}] + \sum_k \sum_{l=k+1}^{\nu} [D_{kl}(\underline{\theta}) E_{kl}^{(D)}] + \mathcal{O}(\sin^3 \delta). \quad (\text{B14})$$

and we have used that $E_k^{(B)} = 0$ due to $g_k = 0$. We now make two observations which pose strict constraints on the geometry of the energy surface around local optima. First, the energy function in this case is (approximately) reflection symmetric via

$$E(\underline{\theta}) = E(-\underline{\theta}) + \mathcal{O}(\sin^3 \delta), \quad (\text{B15})$$

due to the reflection symmetry of the basis functions $A(\underline{\theta})$, $C_k(\underline{\theta})$ and $D_{kl}(\underline{\theta})$. Second, any slice of the energy function is just a shifted cosine function as

$$E(\theta_k v_k) = E^{(A)} (1 + \cos[\theta_k]) / 2 + E_k^{(C)} (1 - \cos[\theta_k]) / 2, \quad (\text{B16})$$

which can be written as $a + b \cos(\theta_k)$ and $a = E^{(A)} + E_k^{(C)}$, while $b = E^{(A)} - E_k^{(C)}$.

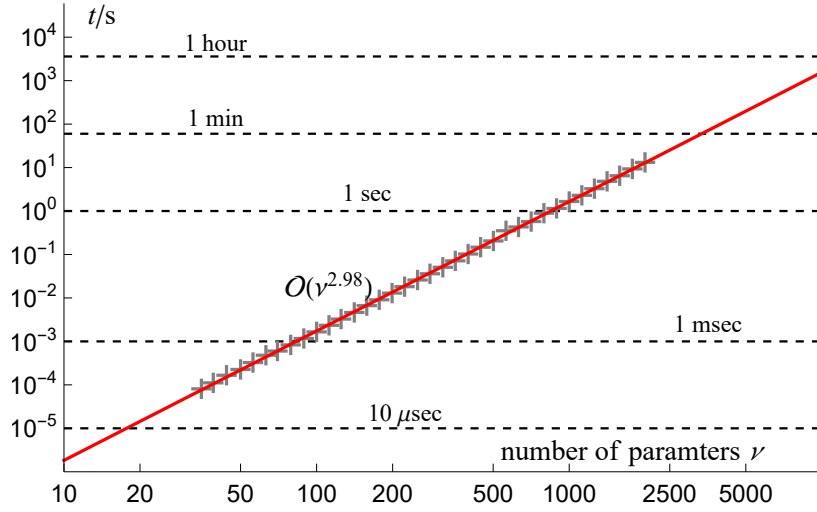


FIG. 3. Classically computing the gradient vector using our efficient C code [43]. Execution times estimated on a laptop for an increasing number of parameters ν confirm the theoretical complexity $\mathcal{O}(\nu^3)$ from Sec. D 1. Descending 1000 steps towards the minimum of the classical function can be performed in a matter of minutes for up to many hundreds of parameters. Our code was executed on a single thread, but the algorithm described in Sec. D 1 could be parallelised.

Appendix C: Expanding the metric tensor entries

It was shown in [29] that the quantum Fisher information matrix can be approximated by the scalar product

$$[\mathbf{F}_Q]_{mn} = 2\text{Tr}\left[\frac{\partial\rho(\underline{\theta})}{\partial\theta_m}\frac{\partial\rho(\underline{\theta})}{\partial\theta_n}\right], \quad (\text{C1})$$

which relation becomes exact in the limit of pure states. Here we have denoted $\rho(\underline{\theta}) := \Phi(\underline{\theta})\rho_0$. We can straightforwardly express the partial derivatives via the partial derivative of the mapping

$$\frac{\partial\rho(\underline{\theta})}{\partial\theta_m} = \frac{\partial\Phi(\underline{\theta})}{\partial\theta_m}\rho_0 = \frac{\partial\tilde{\Phi}(\underline{\theta})}{\partial\theta_m}\rho_0 + \mathcal{O}(\sin^3\delta), \quad (\text{C2})$$

which we aim to express explicitly using our approximate mapping $\tilde{\Phi}(\underline{\theta})$ from Eq. (A13). We can compute the derivative analytically as

$$\frac{\partial\tilde{\Phi}(\underline{\theta})}{\partial\theta_m} = \frac{\partial A(\underline{\theta})}{\partial\theta_m}\Phi^{(A)} + \sum_{k=1}^{\nu}\left[\frac{\partial B_k(\underline{\theta})}{\partial\theta_m}\Phi_k^{(B)} + \frac{\partial C_k(\underline{\theta})}{\partial\theta_m}\Phi_k^{(C)}\right] + \sum_k\sum_{l=k+1}^{\nu}\left[\frac{\partial D_{kl}(\underline{\theta})}{\partial\theta_m}\Phi_{kl}^{(D)}\right] + \mathcal{O}(\sin^2\delta). \quad (\text{C3})$$

and note that this expression is directly analogous to the gradient vector from Eq. (B3), and we have defined the partial derivatives of the monomials, such as $\frac{\partial A(\underline{\theta})}{\partial\theta_m}$, in Sec. B 1. Expanding the quantum Fisher information to leading terms only results in

$$[\mathbf{F}_Q]_{mn} = \mathcal{F}_{BB}F_{BB}(\underline{\theta}) + \mathcal{F}_{AB}F_{AB}(\underline{\theta}) + \cdots + \mathcal{O}(\sin^2\delta). \quad (\text{C4})$$

We do not write out all the terms explicitly for clarity – however, note that they could be computed straightforwardly.

Similarly as before, we have monomials that completely absorb the continuous dependence on the parameters $\underline{\theta}$ and their explicit forms can be computed as

$$F_{BB}(\underline{\theta}) := 2\frac{\partial B_m(\underline{\theta})}{\partial\theta_m}\frac{\partial B_n(\underline{\theta})}{\partial\theta_n} \quad (\text{C5})$$

$$F_{AB}(\underline{\theta}) := 2\frac{\partial B_m(\underline{\theta})}{\partial\theta_m}\frac{\partial A(\underline{\theta})}{\partial\theta_n} + 2\frac{\partial A(\underline{\theta})}{\partial\theta_m}\frac{\partial B_n(\underline{\theta})}{\partial\theta_n} \quad (\text{C6})$$

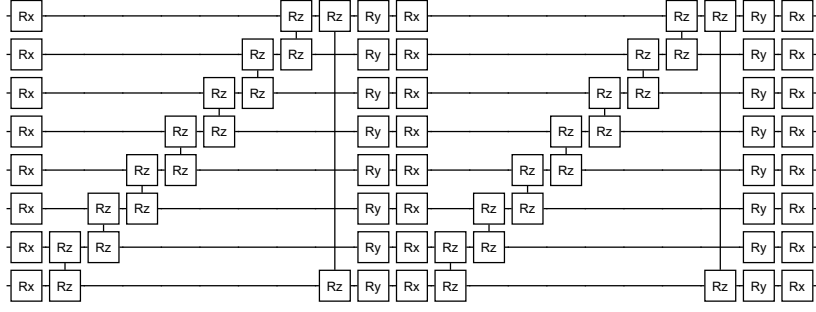


FIG. 4. Example of a 2-block ansatz circuit of 8 qubits. We used 4-block circuits in our simulations.

These functions multiply the coefficients, e.g., $\text{Tr}[(\Phi^{(B)}\rho_0)(\Phi^{(B)}\rho_0)]$, which can be computed via the discrete transformations as

$$\mathcal{F}_{BB} = \text{Tr}[(\Phi^{(B)}\rho_0)(\Phi^{(B)}\rho_0)] = \text{Tr}[\rho(\frac{1}{2}\pi v_k)\rho(\frac{1}{2}\pi v_k)] + \text{Tr}[\rho(-\frac{1}{2}\pi v_k)\rho(-\frac{1}{2}\pi v_k)] \quad (\text{C7})$$

$$- \text{Tr}[\rho(-\frac{1}{2}\pi v_k)\rho(\frac{1}{2}\pi v_k)] - \text{Tr}[\rho(\frac{1}{2}\pi v_k)\rho(-\frac{1}{2}\pi v_k)] \quad (\text{C8})$$

$$\mathcal{F}_{AB} = \text{Tr}[(\Phi^{(A)}\rho_0)(\Phi^{(B)}\rho_0)] = \text{Tr}[\rho(0)\rho(\frac{1}{2}\pi v_k)] - \text{Tr}[\rho(0)\rho(-\frac{1}{2}\pi v_k)]. \quad (\text{C9})$$

The coefficients therefore can be estimated by estimating the overlap between the states, as e.g., $\rho(0)$ and $\rho(\frac{1}{2}\pi v_k)$. These can be straightforwardly estimated using SWAP tests or, in the case of pure states, using Hadamard tests as, e.g.,

$$\text{Tr}[\rho(0)\rho(\frac{1}{2}\pi v_k)] = |\langle\psi(0)|\psi(\frac{1}{2}\pi v_k)\rangle|^2. \quad (\text{C10})$$

Appendix D: Numerical simulations

1. Classical algorithm for computing the gradient vector

We now describe how the analytical gradient from Eq. (B3) can be computed classically efficiently. We assume the the coefficients $E^{(A)}, E_k^{(B)}, E_k^{(C)}, E_{kl}^{(D)}$ are already determined and accessible in RAM. This requires $\mathcal{O}(\nu^2)$ space, which is reasonable for up to thousands of parameters.

First our classical algorithm needs to compute the monomials, e.g., $\frac{\partial A(\theta)}{\partial \theta_m}$ for a given input vector θ . We do this by precomputing and storing the basis functions $a(\theta_k), b(\theta_k) = 1 \pm \cos(\theta_k)$ and $c(\theta_k) = \sin(\theta_k)/2$ and

$$\frac{\partial a(\theta_k)}{\partial \theta_k} = -\sin[\theta_k]/2, \quad \frac{\partial b(\theta_k)}{\partial \theta_k} = \cos[\theta_k]/2, \quad \frac{\partial c(\theta_k)}{\partial \theta_k} = \sin[\theta_k]/2,$$

for all parameters $k \in \{1, \dots, \nu\}$. This can be evaluated in $\mathcal{O}(\nu)$ time and requires $\mathcal{O}(\nu)$ storage space.

In the next step we multiply together the basis functions $a(\theta_k)$ to obtain $A(\theta)$ as

$$A(\theta) = a(\theta_1)a(\theta_2) \cdots a(\theta_\nu),$$

and we store it. All other monomials are obtained from this just by dividing it by, e.g., $a(\theta_k)$, and then multiplying it with, e.g., $\frac{\partial b(\theta_k)}{\partial \theta_k}$, which components we have already precomputed. For example, the monomial $\frac{\partial B_k(\theta)}{\partial \theta_m}$ is obtained as

$$\frac{\partial B_k(\theta)}{\partial \theta_m} = \frac{A(\theta)}{a(\theta_k)a(\theta_m)} \frac{\partial b(\theta_m)}{\partial \theta_m} b(\theta_k),$$

when $k \neq m$ and note that we have already precomputed all components in the above equation. In conclusion, evaluating all $\nu Q = \mathcal{O}(\nu^3)$ basis functions in the gradient vector for a given input vector θ can be done in $\mathcal{O}(\nu^3)$ time and requires $\mathcal{O}(\nu^2)$ storage. We have estimated execution times of our C implementation from [43] which confirms this theoretical complexity, refer to Fig. 3.

2. Simulated optimisation

We use the ansatz circuit structure shown in Fig. 4 in our simulations. This consists of layers of single-qubit X and Y rotations as well as layers of two-qubit Pauli ZZ gates.

In case of Analytic Descent, at every step there is a classical optimisation procedure involved, for which we have used the natural gradient update rule and we aborted the internal loop when the similarity measure is low via $1 - f < 5$. We estimated the metric tensor and inverted it using a large regularisation parameter $\eta = 0.01$ to ensure that its measurement cost is reasonable. The step size is 0.001 (0.1) in the case of analytic descent (natural gradient).

We consider a 6-qubit Hamiltonian of the LiH molecule. We use an ansatz circuit with 4 blocks and overall 78 parameters and start the optimisation at the vicinity of the Hartree-Fock solution. We do so by adding uniform random numbers $(-0.5, 0.5)$ to the initial parameters of the Hartree-Fock solution. The step size is 0.001 (0.1) in the case of analytic descent (natural gradient). We also determine the metric tensor at every iteration step and regularise it with a large $\eta = 0.01$.

We also consider a 12-qubit spin-ring Hamiltonian

$$\sum_{i=1}^N J[\sigma_x^{\{i\}} \sigma_x^{\{i+1\}} + \sigma_y^{\{i\}} \sigma_y^{\{i+1\}} + \sigma_z^{\{i\}} \sigma_z^{\{i+1\}}] + \sum_{i=1}^N \omega_i \sigma_z^{\{i\}},$$

in which we have set $N + 1 = 1$. We randomly generate ω_i and set $J = 0.05$. We use an ansatz circuit of 2 blocks and overall 84 parameters. We start the optimisation from the lowest energy computational basis state by adding uniform random numbers $(-0.5, 0.5)$ to its parameters. The step size is 0.01 (0.01) in the case of analytic descent (natural gradient).

We simulate shot noise when determining the gradient vector (in case of conventional natural gradient) and the coefficients in Eq. (B1). We do so by adding Gaussian distributed random numbers to their exactly determined values, as discussed in the main text.